Magnetochemistry of the tetrahaloferrate(III) ions 6. Crystal structure and magnetic ordering in $[(pyH)_3Cl][FeCl_4]_2$

Roey Shaviv, Carol B. Lowe
Department of Chemistry, University of Illinois at Chicago, Chicago, IL 60680 (USA)

Jalal A. Zora, Christer B. Aakeröy, Peter B. Hitchcock, K. R. Seddon
School of Chemistry and Molecular Science, University of Sussex, Brighton BN1 9QJ (UK)

and Richard L. Carlin*
Department of Chemistry, University of Illinois at Chicago, Chicago, IL 60680 (USA)

Abstract

The crystal structure, magnetic susceptibilities and specific heat of the title compound were determined by X-ray diffraction, susceptometry between 1.2 and 20 K, and adiabatic calorimetry between 1.5 and 39 K, respectively. The material is found to be a canted antiferromagnet with a critical temperature of 2.212 K. A λ-feature in the heat capacity at that temperature and an apparent break in the susceptibility curves are indicative of the manifestation of long-range order. A large degree of short-range order is observed to persist above the critical temperature, however. The compound crystallizes in the orthorhombic space group *Pbca* ($Z=8$, $a=13.040(2)$, $b=15.929(2)$, $c=27.014(5)$ Å and $V=5611.2$ Å^3). Bond lengths average 2.184(5) and 2.185(2) Å for Fe(1)–Cl and Fe(2)–Cl, respectively, within the slightly distorted tetrahedra. Single crystal magnetic susceptibility measurements of the sample show behavior consistent with that of a three-dimensional Heisenberg antiferromagnet with a small ferromagnetic peak whose maximum is identified at 2.00(1) K. This behavior is indicative of sublattice canting. A fit of the data from high temperature series expansions for a Heisenberg $S=5/2$ simple cubic lattice gives $|J|/k_B=0.084(1)$ K with $g=2.00$.

Introduction

As part of an investigation of the magnetic interactions in a series of compounds containing iron(III), we examined the compound of empirical formula $(pyH)_3Fe_2Cl_9$. Once thought to contain the triply-bridged binuclear complex, [tri-μ-chlorobis-trichloroferrate(III)]$^{3-}$ [1], the compound was studied by Earnshaw and Lewis [2] as part of their investigation of the distance dependence of magnetic interactions between metal atoms. The assumption at that time was that the metal–metal interactions in a triply-bridged dimer complex should be stronger than in a similar di- or mono-bridged species. Magnetic susceptibility data measured between 93 K and room temperature were fit to the equation for a binuclear $S=S'=5/2$ interaction [3]:

$$\chi_A=(3K/T)[55+30\exp(10x)+14\exp(18x)+5\exp(24x)+\exp(28x)]/[11+9\exp(10x)+7\exp(18x)+5\exp(24x)+3\exp(28x)+\exp(30x)]+N(\alpha) \quad (1)$$

where $K=N_0g^2\mu_B^2/3k_B$ and $x=-J/k_BT$. The symbols g, N_0, μ_B and k_B represent the spectroscopic splitting factor, Avogadro's number, the Bohr magneton and Boltzmann's constant, respectively; $N(\alpha)$ is the temperature independent paramagnetic term, J is the exchange constant and T the absolute temperature. A good fit of the data to this function was obtained with values of $J/k_B=-1.7$ K, $g=2.09$, and $N(\alpha)$ taken to be zero. This small interaction was interpreted in terms of a distortion of the octahedra on formation of the binuclear complex in such a way as to cause the iron atoms to move apart. Another conclusion was that the chlorine bridging group was not as effective as an oxygen bridge in enhancing the interaction between metals,

*Author to whom correspondence should be addressed.

0020-1693/92/$5.00

since with oxygen a π-bonding mechanism can operate in the M–L–M (metal–ligand–metal) system.

In a later report, Ginsberg and Robin [3] extended the magnetic susceptibility measurements on $(pyH)_3Fe_2Cl_9$ to lower temperatures, and presented optical and Mössbauer spectra of the compound. These data provided evidence to the fact that the iron is present only as tetrahedral $[FeCl_4]^-$. While the two sets of magnetic susceptibility measurements [2, 3] agreed well over the common temperature region, substantial deviation of the data from the theoretical fit to eqn. (1) below liquid nitrogen temperature was found [3] and no fit to the equation over the entire temperature range with any set of J/k_B and g values could be obtained. Between 90 and 298 K, the newer data set was fit to eqn. (1), with $|J|/k_B = 1.6$ K and $g = 2.00$. It was therefore concluded that the observed exchange coupling in $(pyH)_3Fe_2Cl_9$ is simply a weak antiferromagnetic long-range interaction, with a Weiss constant of $\theta = -4$ K, similar to the interaction in $[(C_2H_5)_4N][FeCl_4]$, and not a pairwise metal–metal interaction [3]. No attempt was made to fit the data to any other theoretical magnetic interaction model.

In order to provide further evidence for a non-dimeric structure, the optical thin-film spectrum of the pyridinium compound was compared to its solution spectrum in acetone, and to that of $[(CH_3)_4N][FeCl_4]$ [3]. The spectra were found to be identical, with the optical density in the $[FeCl_4]^-$ bands of $(pyH)_3Fe_2Cl_9$ twice that of an equimolar solution of $[(CH_3)_4N][FeCl_4]$. The magnitude of the isomer shift for $(pyH)_3Fe_2Cl_9$ in the Mössbauer spectrum was closer to that of the tetrahedral $[(CH_3)_4N][FeCl_4]$ than that for iron(III) chloride, which has octahedral coordination.

Recent studies of magnetic exchange interactions in a set of isostructural compounds with the stoichiometry $A_3Fe_2X_9$ (A = [4-X(py)H]$^+$, X = Cl or Br), have revealed canted antiferromagnetism for substances containing discrete metal ion complexes [4]. The telling weak ferromagnetic peak occurs in the magnetic susceptibility data for measurements in which the applied field is directed perpendicular to the easy axis along a crystallographic axis, namely *b*, for these nominally antiferromagnetic materials.

It will be seen from our X-ray results that $(pyH)_3Fe_2Cl_9$ does indeed contain discrete $[FeCl_4]^-$ ions, but is not isostructural with the other $A_3Fe_2X_9$ compounds previously reported [4–7]. The magnetic measurements show that the antiferromagnetic exchange is weak in $(pyH)_3Fe_2Cl_9$, for it orders at only 2.212 K, but evidence of canting is still present. The magnetic susceptibility measurements for the pyridinium compound reveal a weak ferromagnetic contribution along the *c* crystallographic direction, unlike in the 4-halo-substituted pyridinium compounds [4]. This report contains the synthesis, complete crystal structure, and single crystal and powder magnetic susceptibility studies for $[(pyH)_3Cl][FeCl_4]_2$, with a calculated theoretical fit of the magnetic data obtained and a look at the plausible superexchange paths. The critical temperature for long-range order and the extent of short-range order are best determined by specific heat measurements. No previous such measurements of this compound have been reported. Thus the specific heat of the title compound was also measured between 1.5 and 39 K using adiabatic calorimetry.

Experimental

Preparation of $[(pyH)_3Cl][FeCl_4]_2$

The method of preparation was similar to that used by Weinland and Kiszling [1]. Anhydrous iron(III) chloride or iron(III) chloride hexahydrate and pyridinium chloride were each dissolved in dilute hydrochloric acid and then mixed together (molar ratio 1:2). The yellow–brown solution was placed over conc. H_2SO_4 at room temperature and produced large prismatic single crystals after 4 to 6 days. The yellow–green hygroscopic crystals were then collected by filtration, and dried *in vacuo*. *Anal.* Calc. for $C_{15}H_{18}Cl_9Fe_2N_3$: C, 26.85; H, 2.70; Cl, 47.55; Fe, 16.64; N, 6.26. Found: C, 27.03; H, 2.67; Cl, 47.47; Fe, 16.31; N, 6.20%.

Crystal alignment procedures

Crystals (25–80 mg) for magnetic susceptibility measurements were chosen and aligned using a polarizing microscope. Smaller crystals suitable for X-ray analysis were also aligned by X-ray precessional photographic methods. The single crystals were sealed with a thin layer of Apiezon N grease before mounting in the

TABLE 1. Crystallographic data for $[(pyH)_3Cl][FeCl_4]_2$

Chemical formula	$C_{15}H_{18}Cl_9Fe_2N_3$
Formula weight (g/mol)	671.1
Crystal class	orthorhombic
Space group	*Pbca*
Sample temperature (°C)	25
a (Å)	13.040(2)
b (Å)	15.929(2)
c (Å)	27.014(5)
V (Å^3)	5611.3
Z	8
λ (Å)	0.71069
ρ_{calc} (g cm^{-3})	1.59
μ (Mo Kα) (cm^{-1})	19.1
Structure solution package	MULTAN
Thermal parameters	anisotropic on all non-H atoms
$R(F)$	0.053
$R_w(F^2)$	0.063
Total reflections measured	4565
$\|F^2\| \leq \sigma(F^2)$	2248

TABLE 2. Fractional atomic coordinates ($\times 10^4$) for $[(pyH)_3Cl][FeCl_4]_2$ with e.s.d.s given in parentheses and fractional atomic coordinates for hydrogen atoms ($\times 10^3$) introduced at calculated positions

Atom	x	y	z
Fe(1)	8456.0(9)	162.5(7)	7440.9(4)
Fe(2)	2993.1(8)	2536.8(7)	5040.8(4)
Cl(1)	8023.5(18)	−931.5(14)	6994.8(10)
Cl(2)	8017.1(18)	1283.6(14)	7022.4(9)
Cl(3)	10113.1(17)	177.3(17)	7564.2(9)
Cl(4)	7721.1(19)	157.6(21)	8160.7(9)
Cl(5)	2223.8(16)	1498.5(13)	5418.0(8)
Cl(6)	2609.0(18)	3748.5(13)	5372.5(9)
Cl(7)	4651.5(16)	2331.4(13)	5071.3(9)
Cl(8)	2557.6(20)	2520.6(15)	4261.8(8)
Cl(9)	5755.1(19)	7524.0(14)	3365.6(9)
N(1)	4983(5)	5982(4)	3947(2)
C(2)	5429(6)	5396(5)	3705(3)
C(3)	5273(7)	4604(5)	3820(3)
C(4)	4655(7)	4403(5)	4201(4)
C(5)	4189(6)	5021(6)	4460(3)
C(6)	4368(6)	5824(5)	4329(3)
N(7)	5092(5)	9153(4)	3875(2)
C(8)	4109(6)	9141(6)	3795(3)
C(9)	3508(6)	9705(6)	4012(4)
C(10)	3924(7)	10293(6)	4302(4)
C(11)	4954(8)	10301(5)	4386(3)
C(12)	5548(6)	9724(6)	4168(3)
N(13)	4800(7)	7342(4)	2327(2)
C(14)	3867(8)	7593(6)	2208(4)
C(15)	3531(7)	7476(7)	1742(6)
C(16)	4186(11)	7168(7)	1430(4)
C(17)	5128(11)	6939(7)	1568(3)
C(18)	5389(6)	7031(6)	2007(4)
H(N1)	508	654	386
H(2)	589	554	344
H(3)	561	417	364
H(4)	456	383	429
H(5)	374	490	473
H(6)	405	627	451
H(N7)	550	874	373
H(8)	382	874	357
H(9)	278	970	396
H(10)	352	1072	446
H(11)	526	1072	459
H(12)	627	972	422
H(N13)	502	740	267
H(14)	341	786	244
H(15)	286	758	162
H(16)	406	708	109
H(17)	567	671	134
H(18)	605	688	212

susceptometer, to protect them from moisture. Powder samples (about 100 mg) were obtained by grinding small single or poly-crystals with a mortar and pestle in a dry atmosphere. In some cases the powder sample was further dried using a vacuum line. Magnetic susceptibility measurements in the temperature ranges 1.4–4.2 K and 2.0–25 K proceeded as described earlier [4].

Crystal structure

Room temperature X-ray data was collected using an Enraf-Nonius CAD4 diffractometer in a θ–2θ mode for a crystal of dimensions $0.25\times0.20\times0.18$ mm. Unit cell and refinement parameters are listed in Table 1. A total of 4565 reflections was measured for $2<\theta<23°$, $+h$, $+k$, $+l$; and 2248 unique reflections with $|F^2|>\sigma(F^2)$ were used in the refinement. No crystal decay was observed and no absorption correction was made.

The Fe and Cl atoms were located by direct methods using MULTAN, and the C and N atoms were found on difference maps. Refinement was by full matrix least-squares with anisotropic temperature factors, except for the H atoms which were held fixed at calculated positions (C–H and N–H at 0.95 Å) with B_{iso} of 6.0 Å^2. The weighting scheme was $w=1/\sigma^2(F)$ and the final residuals were $R=0.053$ and $R'=0.063$. A final difference map was featureless. Programs used were from the Enraf-Nonius SDP-Plus package. Fractional atomic coordinates with their standard deviations and isotropic temperature factors are given in Table 2. The associated anisotropic thermal parameters are included in Table 3.

TABLE 3. Thermal parameters ($\times 10^3$) for $[(pyH)_3Cl][FeCl_4]_2$ in the form: $\exp[-2p^2(U_{11}h^2a^{*2}+U_{22}k^2b^{*2}+U_{33}l^2c^{*2}+2U_{12}hka^*b^*+2U_{13}hla^*c^*+2U_{23}klb^*c^*)]$

Atom	U_{11}	U_{22}	U_{33}	U_{12}	U_{13}	U_{23}
Fe(1)	57(1)	80(1)	87(1)	−3(1)	1(1)	2(1)
Fe(2)	61(1)	58(1)	81(1)	−2(1)	6(1)	−2(1)
Cl(1)	102(2)	80(1)	143(2)	−9(1)	−10(2)	−12(1)
Cl(2)	105(2)	78(1)	123(2)	−2(1)	−15(2)	9(1)
Cl(3)	59(1)	150(2)	116(2)	4(1)	−3(1)	−15(2)
Cl(4)	86(2)	209(3)	96(2)	−20(2)	16(1)	6(2)
Cl(5)	78(1)	79(1)	103(2)	−14(1)	2(1)	15(1)
Cl(6)	96(2)	71(1)	128(2)	9(1)	20(1)	−17(1)
Cl(7)	61(1)	83(1)	124(2)	−1(1)	5(1)	−14(1)
Cl(8)	111(2)	115(2)	82(1)	0(2)	−10(1)	10(1)
Cl(9)	111(2)	70(1)	102(1)	2(1)	11(1)	−8(1)
N(1)	81(4)	57(4)	107(5)	0(4)	−9(4)	−2(4)
C(2)	80(5)	96(6)	83(5)	9(5)	12(5)	3(5)
C(3)	121(7)	75(5)	123(7)	26(6)	18(6)	−12(6)
C(4)	117(7)	66(5)	142(8)	−8(6)	−3(7)	29(5)
C(5)	80(6)	133(8)	100(6)	−18(6)	18(5)	13(6)
C(6)	69(5)	106(6)	101(6)	14(5)	5(5)	−41(5)
N(7)	104(5)	67(4)	99(5)	26(4)	21(4)	−2(4)
C(8)	83(6)	97(6)	125(7)	−24(5)	5(6)	−21(6)
C(9)	64(5)	125(7)	148(8)	15(6)	1(6)	−24(7)
C(10)	115(7)	79(6)	161(8)	31(5)	47(6)	−13(6)
C(11)	130(8)	73(5)	100(6)	−6(6)	−2(6)	−21(5)
C(12)	66(5)	115(7)	102(6)	7(5)	−12(5)	6(6)
N(13)	143(7)	75(5)	89(5)	3(5)	−8(5)	−7(4)
C(14)	149(8)	95(7)	171(8)	13(6)	88(6)	−8(7)
C(15)	68(5)	97(7)	335(16)	8(6)	−47(8)	23(9)
C(16)	325(14)	100(7)	161(8)	−55(9)	−144(8)	21(7)
C(17)	252(13)	171(9)	91(6)	−5(10)	35(8)	−77(6)
C(18)	71(6)	92(6)	215(10)	7(5)	5(7)	−54(7)

Specific heat

Heat capacity measurements were carried out in an adiabatic calorimetric cryostat. The experimental apparatus and pertinent operating techniques have been previously described [8]. The polycrystalline sample was ground with a mortar and pestle and pelleted, into two pellets, to fit the inside of the calorimeter. Rapid thermal equilibrium was facilitated by threading the pellets with about 0.5 g of fine copper wire. Thermal contact between the pellets and the gold plated OFHC copper calorimetric vessel was provided by a thin layer of Apiezon N grease. The sample used was synthesized especially for the calorimetric experiment and was not the same sample used in the determination of the magnetic susceptibilities. In all about 12.25 g samples were used, which correspond to 0.01825 mol, when 671.101 g/mol is selected as the molecular mass.

During the course of the experiment 100 data points were taken using the standard heat pulse technique. Thermal equilibrium time, for each individual point, was between 3 and 6 min. The precision of a single point was better than 0.1% above the transition region and about 0.7% below it, where temperature increments were significantly smaller.

Results and discussion

Crystal lattice structure

One molecular formula contains three pyridinium cations, two $[FeCl_4]^-$ tetrahedra and one chloride ion which is strongly bonded to the three pyridinium cations. Intramolecular bond distances and angles are shown in Table 4. The two separate tetrachloroferrate(III) groups describe slightly distorted tetrahedra, with an average of 2.184 Å for Fe(1)–Cl bond lengths and 2.185 Å for the corresponding Fe(2)–Cl lengths. These values are comparable with those reported earlier [4] (literature mean = 2.175(9)). Bond angles for Cl–Fe–Cl within the anions range from 107.0 to 112.1°, with the normal tetrahedral average of 109.5°. In this material the tetrahedra are not aligned with two- or three-fold axes parallel to any crystallographic axis, as with some other tetrahaloferrate(III) structures [4–7].

With $Z = 8$, the 16 $[FeCl_4]^-$ tetrahedra in each unit cell form four two-dimensional layers which are roughly perpendicular to the *c* axis. Two-dimensional magnetic ordering seen in many layer-type structures is not expected in this case, because the inter-layer separation is only 6.75 Å. This distance is not very different from the shortest Fe- - -Fe distance of 6.53 Å found along the *a* direction within the planes. A sketch showing relative Fe- - -Fe distances within the unit cell and the tetrahedral staggered ABAC layer stacking is given in Fig. 1. Between-layer Fe- - -Fe contacts shown in the drawing range from 7.808 to 8.188 Å. Within the A layers the Fe- - -Fe distances along the *b* direction are 8.562 Å, however within the B and C layers adjacent ferric ions along *b* are 8.831 Å distant. Overall three-dimensional magnetic order is predicted for $(pyH)_3Fe_2Cl_9$. However, with very favorable superexchange paths lacking, the transition is likely to occur at low temperatures. No such transition was reported earlier [3] though the magnetic susceptibility measurements span the temperature range from 298 down to 1.4 K. On the other hand, our results indicate a transition at about 2 K. We will show that this apparent discrepancy arises from the fact that the temperature increments between the data points measured by Ginsberg and Robin near the critical temperature region (at 1.4 and 4.2 K) are too large.

Within the pyridinium rings, bond distances and angles are normal, with averages of *r*(C–N) 1.31, *r*(C–C) 1.33 Å, and (∠s) 119.9 ± 4°, respectively. The three pyridinium rings depicted in Fig. 2 are arranged in propeller-like fashion about the free halide. Short H- - -Cl contacts between nitrogen bound H atoms and

TABLE 4. Intramolecular distances (Å) and angles (°) for $[(pyH)_3Cl][FeCl_4]_2$ with e.s.d.s given in parentheses

Distances (Å)			
Fe(1)–Cl(1)	2.192(3)	Fe(1)–Cl(2)	2.190(3)
Fe(1)–Cl(3)	2.187(2)	Fe(1)–Cl(4)	2.168(3)
Fe(2)–Cl(5)	2.186(2)	Fe(2)–Cl(6)	2.186(2)
Fe(2)–Cl(7)	2.189(2)	Fe(2)–Cl(8)	2.180(2)
N(1)–C(2)	1.280(10)	N(1)–C(6)	1.331(10)
C(2)–C(3)	1.315(12)	C(3)–C(4)	1.347(13)
C(4)–C(5)	1.352(13)	C(5)–C(6)	1.348(13)
N(7)–C(8)	1.301(11)	N(7)–C(12)	1.345(11)
C(8)–C(9)	1.329(13)	C(9)–C(10)	1.337(13)
C(10)–C(11)	1.362(13)	C(11)–C(12)	1.339(12)
N(13)–C(14)	1.320(13)	N(13)–C(18)	1.257(13)
C(14)–C(15)	1.35(2)	C(15)–C(16)	1.30(2)
C(16)–C(17)	1.34(2)	C(17)–C(18)	1.242(15)
Cl(9)–H(1)	2.23	Cl(9)–H(7)	2.20
Cl(9)–H(13)	2.12		
Angles (°)			
Cl(1)–Fe(1)–Cl(2)	107.3(1)	Cl(1)–Fe(1)–Cl(3)	110.3(1)
Cl(1)–Fe(1)–Cl(4)	112.1(1)	Cl(2)–Fe(1)–Cl(3)	109.2(1)
Cl(2)–Fe(1)–Cl(4)	110.5(1)	Cl(3)–Fe(1)–Cl(4)	107.5(1)
Cl(5)–Fe(2)–Cl(6)	111.83(9)	Cl(5)–Fe(2)–Cl(7)	108.83(9)
Cl(5)–Fe(2)–Cl(8)	108.7(1)	Cl(6)–Fe(2)–Cl(7)	110.1(1)
Cl(6)–Fe(2)–Cl(8)	110.3(1)	Cl(7)–Fe(2)–Cl(8)	107.0(1)
C(2)–N(1)–C(6)	122.1(7)	N(1)–C(2)–C(3)	120.7(8)
C(2)–C(3)–C(4)	120.0(8)	C(3)–C(4)–C(5)	119.5(8)
C(4)–C(5)–C(6)	118.5(8)	N(1)–C(6)–C(5)	119.2(8)
C(8)–N(7)–C(12)	123.0(7)	N(7)–C(8)–C(9)	119.8(8)
C(8)–C(9)–C(10)	119.6(8)	C(9)–C(10)–C(11)	120.3(8)
C(10)–C(11)–C(12)	119.4(8)	N(7)–C(12)–C(11)	117.9(8)
C(14)–N(13)–C(18)	121.1(9)	C(13)–C(14)–C(15)	118.9(9)
C(14)–C(15)–C(16)	116.0(1)	C(15)–C(16)–C(17)	122.0(1)
C(16)–C(17)–C(18)	119.0(1)	N(13)–C(18)–C(17)	122.0(1)
H(1)–Cl(9)–H(7)	107	H(1)–Cl(9)–H(13)	106
H(7)–Cl(9)–H(131)	114		

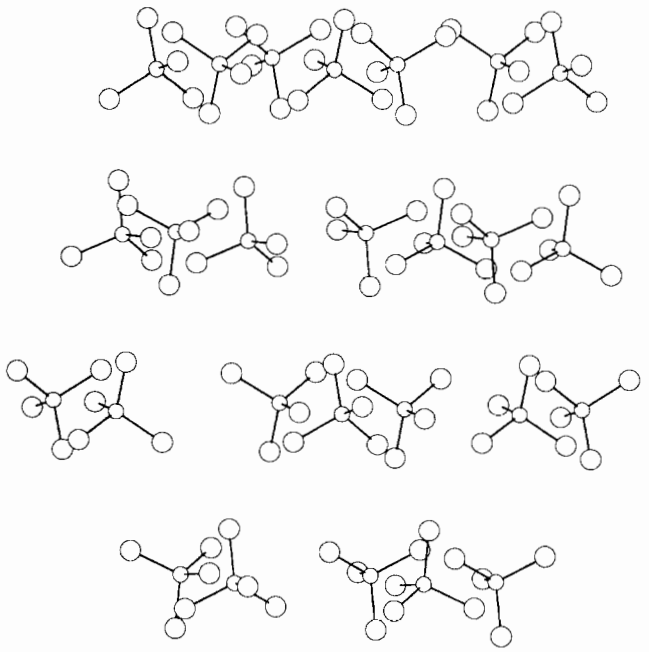

Fig. 1. The packing of the tetrahedra in the orthorhombic unit cell of $[(pyH)_3Cl][FeCl_4]_2$. The layers are shown successively in the order CABA.

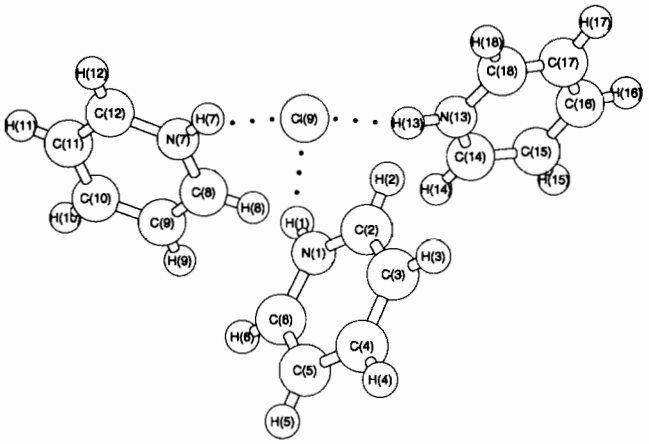

Fig. 2. Hydrogen bonding and pyridinium ion arrangement in the $[(pyH)_3Cl]^{2+}$ cation.

Cl(9) averaging 2.18 Å, disclose strong H bonding. The average N–H- - -Cl distance is 3.076 Å, close to values given [9] for hydrazinium(2+) dichloride (3.10±0.02 Å) and hydroxylaminium(1+) chloride (3.16±0.02 Å). A range of H- - -Cl(9)- - -H angles between 106 and 114° indicate near tetrahedral H-bond coordination to Cl(9). The discrete nature of the strong hydrogen bonds to the chloride ion leads to the recognition of the cation $[(pyH)_3Cl]^{2+}$, similar to that observed in the 4-chloropyridinium analogue [4]. This stable entity completes the tetrahedral coordination sphere around the chloride ion by the formation of a weak hydrogen bond (r(H ... Cl)2.746 Å) to an H3 proton of a neighboring $[(pyH)_3Cl]^{2+}$ cation, thus forming a three-dimensional hydrogen-bonded cationic network. There are no hydrogen bonds between $[(pyH)_3Cl]^{2+}$ and the $[FeCl_4]^-$ units.

The individual hydrogen bonds in the $[(pyH)_3Cl]^{2+}$ cation are longer than those in pyridinium chloride (r(N ... Cl) 2.95 Å) [10], reflecting the charge depletion at the chloride center when it receives four hydrogen bonds.

Zero-field magnetic susceptibilities

The zero-field susceptibility data with the *ac* field H (ν=155 Hz) aligned along the crystal a, b and c axes are shown in Fig. 3. No correction for demagnetization was required for the small values of the susceptibility. Single crystal data are shown for temperatures between 1.1 and 4.2 K and measurements of polycrystalline powder are shown for the temperature range 1.1–24 K. It is clear that the material undergoes long range three-dimensional antiferromagnetic order at about 2 K. An out-of-phase component χ'' was detected between approximately 1.5 to nearly 2.1 K. The susceptibility increases as temperatures drop and attains a maximum value of 0.55 emu mol^{-1} at T=2.3 K. A second maximum is seen in the data at T=2.00 K as the development of weak ferromagnetic alignment occurs, corresponding to the χ'' observation. Below this temperature the susceptibility decreases, but does not extrapolate to zero for T=0 K for any of the $H\|a$, b, c measurements. For an orthorhombic crystal the easy axis must follow one of the crystallographic axes, determined only experimentally [11]. The data which approach the smallest values of χ are the values measured for $H\|a$, indicating that the easy axis is probably coincident with the a axis direction, with deviation due to misalignment of

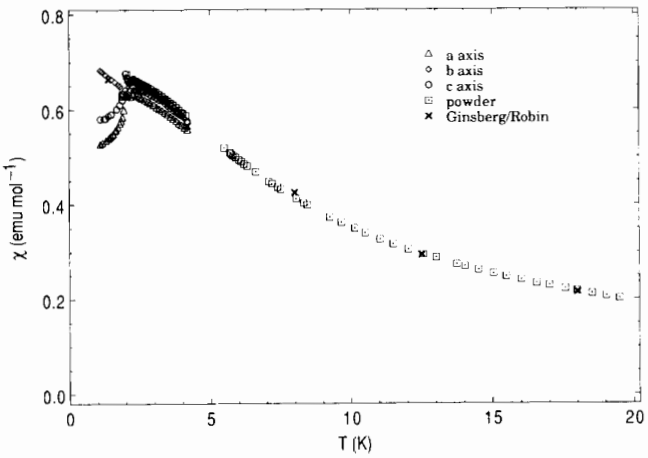

Fig. 3. The magnetic susceptibility curves for $(pyH)_3Fe_2Cl_9$. The measurements along the a, b and c axes are illustrated by triangles, diamonds and circles, respectively; powder data are represented by squares. The lowest temperature data of Ginsberg and Robin [3] are shown as ⧗.

the crystal or some impurity. Misalignment is not unlikely, as we note a small component of the weak ferromagnetic peak in data measured with the field along the *a* direction as well. An impurity which might cause an increase in the susceptibility below T_c could be a very small amount of $(pyH)_5Fe_2Cl_{11}$, which we have found does not order above 1.1 K.

From the present data it may be concluded that the compound orders as a canted antiferromagnet. With the moments aligned toward the *a* axis, canting occurs toward the *c* axis with a very small net moment along *c*. Since tetrahedral iron(III) salts generally have isotropic *g* values with small zero field splitting and spin orbit coupling effects, the Heisenberg model will apply here. Three-dimensional ordering is clearly present from the susceptibility data and we use a high temperature series expansion [12] to fit the data. In this way we obtain an adequate fit with $g=2.02$, and $J/k_B = -0.084(1)$ K. The fit is based on a simple cubic lattice with six nearest neighbors. This is a reasonable lattice approximation if the important interactions shown in Fig. 1 are those parallel to *a* and those running diagonally between tetrahedra in the *bc* plane. It is not known whether the pyridinium rings increase magnetic isolation along any of the pathways pictured.

The data presented here are in basic agreement with those of Ginsberg and Robin [3]. The presence of three-dimensional order was not noted by the earlier studies due to the lack of data at low enough temperatures, and the infrequency of the data points measured. Curie–Weiss plots of the three data sets yield θ values of -4, 8 and -4 K for the Ginsberg and Robin, Earnshaw and Lewis and the present data, respectively. The close agreement in the Weiss constant for two of the data sets is gratifying, given the variation in temperature regions measured. A very good fit to the high temperature series expansion for the $S=5/2$ sc Heisenberg model was obtained using the three data sets combined over the large temperature span of 3 to 300 K (Fig. 4). Parameters obtained for the combined data were $g=2.00$ and $J/k_B = -0.084(1)$ K.

The theoretical predictions given below are a good reference as to how well this compound behaves as a simple cubic $S=5/2$ Heisenberg antiferromagnet. According to Puertolas *et al.* [13]

$$\chi_{max}|J|/N_0g^2\mu_B^2 = 0.0394(1) \quad (2)$$

$$k_BT(\chi_{max})/|J|S(S+1) = 3.07(1) \quad (3)$$

$$k_BT_c/|J|S(S+1) = 2.84(1) \quad (4)$$

where all of the parameters have their previously defined meanings. Substituting our experimental values for χ_{max}, $T(\chi_{max})$, T_c, and that of $|J|/k_B$ obtained from our high temperature series fit, we calculate ratios of parameters for eqns. (2) through (4) of 0.0379, 3.01 and 3.14,

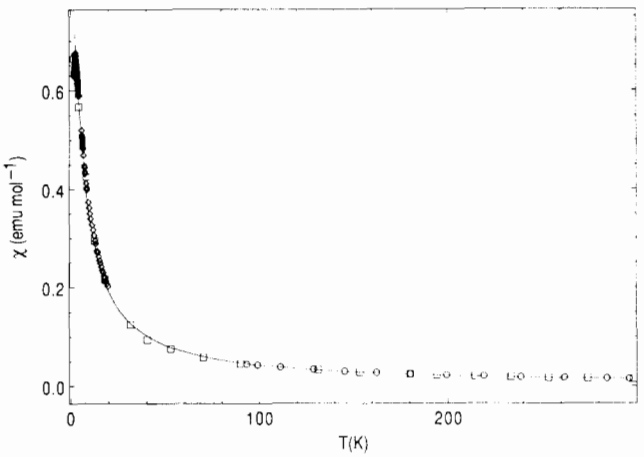

Fig. 4. Comparison of magnetic susceptibility measurements from three sources. The circles are data taken by Earnshaw and Lewis [2], the squares are from Ginsberg and Robin [3] and the diamonds are from this work. The solid line is a theoretical fit, explained in the text.

respectively. Though it appears contradictory because of the weak ferromagnetism, the presence of which implies a certain degree of anisotropy, the substance appears to follow the Heisenberg model quite well. The physical significance of this argument is questionable, however, in light of the complex nature of the magnetic susceptibility near the critical temperature. The two maxima observed in the data and the fact that the susceptibility may not be extrapolated to zero at 0 K for any of the axes strongly suggests that the nature of the magnetic interactions is complicated and may not be accounted for by a simple model.

Two mechanisms have been previously proposed to account for weak ferromagnetism [14]. One involves single ion anisotropy and the other mechanism involves anisotropic spin–spin coupling. The second mechanism is operative in the canted antiferromagnet α-Fe_2O_3 and we consider this further.

For antisymmetric spin couplings to exist, certain requirements are necessary. In all cases the symmetry must be sufficiently low. Moriya gives rules for determining when *d*, the coupling constant vector between two ions A and B, is non-zero and also for determining its possible directions [14]. Following these rules for this orthorhombic system with space group *Pbca*, we can make the following observations based on symmetry. (i) It is readily evident from Fig. 1 that no inversion center exists between neighboring Fe(III) tetrahedral ions along the *a*, *b* or *c* axes. This means that *d* may be non-zero for this crystal space group. There is, however, inversion symmetry between tetrachloroferrate(III) ions along the face diagonals in the *a*–*b* plane. Consequently no canting is allowed between these sites. (ii) There is a mirror plane separating adjacent ions along the *b* crystallographic direction. This effectively

TABLE 5. Molar heat capacities of bis[pyridinium tetrachloroferrate(III)]·pyridinium chloride (M=671.101 g mol^{-1})

T (K)	$C_{p,m}/R$[a]	T (K)	$C_{p,m}/R$	T (K)	$C_{p,m}/R$	T (K)	$C_{p,m}/R$	T (K)	$C_{p,m}/R$
Series I		2.013	3.4095	1.998	3.0486	4.760	0.9356	13.961	4.9629
1.575	2.0196	2.046	3.4724	2.038	3.3419	5.039	0.9323	14.678	5.4342
1.601	1.9858	2.080	3.6223	2.071	3.6785	5.324	0.9452	15.438	5.9429
1.639	1.8252	2.113	3.7807	2.099	3.7416	5.616	0.9735	16.232	6.4871
1.684	2.0439	2.144	3.9885	2.126	3.8423	5.919	1.0190	17.070	7.0704
1.755	2.3311	2.173	4.1722	2.152	4.0269	6.238	1.0831	17.946	7.6911
1.843	2.6425	2.202	4.2236	2.176	4.2140	6.568	1.1608	18.879	8.3461
1.921	2.9292	2.231	3.9125	2.198	4.3908	6.921	1.2608	19.860	9.0368
1.990	3.2845	2.265	3.1751	2.221	4.1836	7.287	1.3763	20.893	9.7686
2.052	3.5480	2.307	2.8620	2.312	2.9501	7.667	1.5102	21.979	10.5354
2.135	3.9342	2.352	2.5935	2.465	2.1540	8.062	1.6621	23.128	11.3195
		2.401	2.3823	2.606	1.9385	8.473	1.8373	24.334	12.1177
Series II		2.452	2.2013	2.750	1.6637	8.906	2.0331	25.599	12.9734
1.629	2.1664	2.516	2.0743	2.939	1.5090	9.361	2.2508	26.926	13.9095
1.677	2.0213			3.131	1.3479	9.840	2.4948	28.235	14.8947
1.739	2.2644	Series III		3.324	1.2386	10.346	2.7661	29.643	15.9389
1.801	2.5271	1.712	2.1462	3.541	1.1461	10.868	3.0599	31.206	17.0227
1.852	2.6780	1.785	2.4819	3.754	1.0820	11.427	3.3886	32.844	18.0676
1.898	2.8449	1.846	2.6556	4.004	1.0168	12.013	3.7367	34.595	19.1045
1.938	2.9995	1.901	2.8500	4.260	0.9722	12.634	4.1135	36.424	20.1404
1.977	3.2314	1.951	3.0771	4.496	0.9465	13.280	4.5238	38.358	21.1264

[a]R=8.3144 J K^{-1} mol^{-1}.

confines the d term in $d[S_i x S_j]$ to be parallel to the a–c plane. The value of d is estimated to be of the order of $\Delta g/g$ times the superexchange interaction, where $\Delta g = g - 2$. This value can be very small, for example $\Delta g/g \approx 1 \times 10^{-3}$ in α-Fe_2O_3 [15]. Susceptibility measurements indicate that the easy axis is probably along a. Therefore, a d term along c would meet all symmetry requirements and remain perpendicular to the easy axis, effectively causing the spins to tilt slightly away from the a axis toward c. A net moment would then be observable along the c direction for a simple two-sublattice system [16].

Specific heat

The experimental molar specific heat of $[(pyH)_3Cl][FeCl_4]_2$ along with the sample's thermal history during the course of the calorimetric experiment are listed in Table 5 and plotted in Fig. 5. The experimental heat capacity is the sum of the lattice and the excess contributions. In $[(pyH)_3Cl][FeCl_4]_2$, all excess heat capacity may be assigned to the magnetic ordering process. A resolution of this heat capacity contribution from the experimental results depends upon a successful resolution of the latter to lattice and excess contributions.

The magnetic and lattice heat capacities were resolved by means of the enhanced Komada/Westrum (KW) method in a manner that was described in the preceding papers in this series [8, 17]. Thus the apparent characteristic temperature θ_{KW} (Fig. 6) was determined over

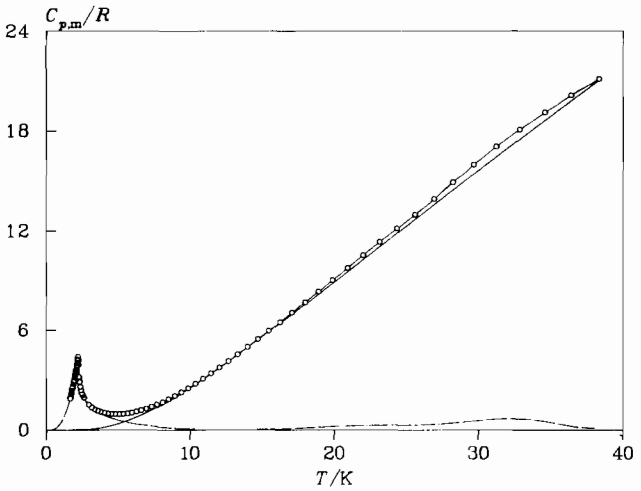

Fig. 5. Specific heat of $[(pyH)_3Cl][FeCl_4]_2$: O–O–O, experimental results; ——, lattice heat capacity; – – –, magnetic heat capacity.

the entire temperature range of the experiment, 26.25 K was assigned as the characteristic temperature for the compound and the lattice heat capacity (Fig. 5) was evaluated on the basis of this value. A minimum in the apparent characteristic temperature is observed at the vicinity of 2 K and a second local minimum is present near 32 K. The two minima are reflected in the two maxima in the magnetic heat capacity (calculated by subtracting the lattice contribution from the experimental data) and are associated with long- and short-range ordering, respectively. The long-range mag-

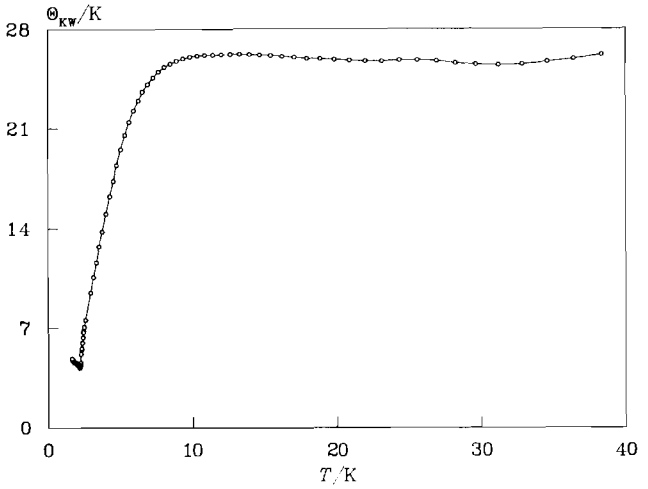

Fig. 6. Apparent characteristic temperature, θ_{KW}, for the title compound.

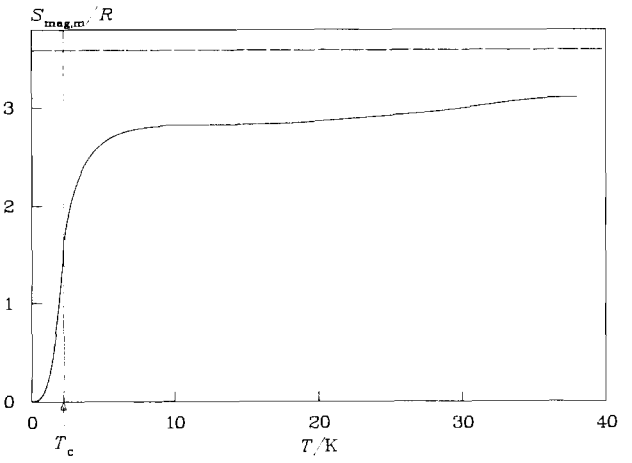

Fig. 7. Magnetic entropy of $[(pyH)_3Cl][FeCl_4]_2$. The critical temperature, 2.212 K, is indicated by the solid vertical line. The upper limit for the magnetic entropy, 3.5835R, is indicated by the horizontal dashed line.

netic order gives rise to a λ-feature in the magnetic heat capacity, whose maximum is identified at 2.212 K, which is selected as the critical temperature (Fig. 5). The low temperature segment of the transition does not follow the behavior predicted by spin wave theory as the magnetic heat capacity increases almost linearly with temperature between 1.6 and 2.0 K. The magnetic heat capacity below the critical temperature was extrapolated to 0 K by using the data between 1.6 and 1.8 K to produce a distribution function which was, in turn, used to reproduce the magnetic heat capacity over that range. The same distribution function was then used to extrapolate the heat capacity curve from 1.6 to 0 K, under the constraint of a T^3 dependence approaching absolute zero temperature. A polynomial fit between 0 K and the critical temperature yielded $1.518R$ for the magnetic entropy at the critical temperature. This value is only 42% of the total theoretical magnetic entropy of $3.584R$. The fact that less than half of the magnetic ordering takes place below the critical temperature indicates that short-range phenomena play an important role in the magnetic ordering process.

Short-range order manifests itself with a broad maximum in the vicinity of 31.5 K. Only about a third of the ordering entropy is associated with short-range order. This may explain the lack of evidence for short-range order in the magnetic susceptibility data. The experimental data do not extend to high enough temperatures to allow a complete analysis of the short-range contribution. We cannot, therefore, be certain about the exact exchange pathways responsible for the phenomena. We note, however that anticipated short-range order provided the original motivation for the study of this material [2, 3]. The conclusion that the compound is a simple antiferromagnet should be revised in light of these data. Short-range order is found to be a common feature in this series of tetrahaloferrates(III). Thus, $(pyH)_3Fe_2Br_9$ displays short-range order while $[4\text{-}Br(py)H]_3Fe_2Cl_9$ has the ordering phenomena equally divided between short- and long-range order. Of the materials studied in this chemical system to date, only $[4\text{-}Cl(py)H]_3Fe_2Cl_9$ does not display an important degree of short-range order.

The critical temperature, as identified by the specific heat experiment appears about 0.21 K higher than the temperature at which the weak ferromagnetic peak in the magnetic susceptibility is identified. However, at the vicinity of the critical temperature, the resolution of the magnetic susceptibility experiment is not sufficient to provide an unequivocal interpretation of the data. The ordering process appears to result in at least two maxima in the susceptibility data between 2 and 2.3 K. This indicates that the magnetic interactions, on the microscopic scale, are complex and may not be reproduced by a simple model. The atypical shape of the magnetic heat capacity over that temperature region, i.e. the almost zero curvature, reaffirms this observation. The critical temperature, 2.212 K, was, therefore, identified solely on the basis of the maximum in the magnetic heat capacity. We note, however, that the two measurements were not made on the same sample. Small differences in impurity levels and thermal history may also account for the difference in the critical temperatures.

The excess entropy over the entire temperature region of the experiment is $3.09R$ (Fig. 7). This value represents the entropy associated with the long-range order and the portion of the entropy associated with the short-range order that lies in the experimental temperature range. Thus only about 86% of the total magnetic entropy is within our range.

Conclusions

The compound $(pyH)_3Fe_2Cl_9$ behaves as a canted antiferromagnet with very weak exchange. Canting appears to be towards the *c* axis when the *a* axis is identified as the easy axis. The exchange interactions in this compound are among the weakest yet found for these tetrachloroferrates(III), with the possible exception of $(pyH)_5Fe_2Cl_{11}$, which has not yet been fully characterized. It is notable that $(pyH)_3Fe_2Cl_9$ and its counterpart, $(pyH)_5Fe_2Cl_{11}$, are the only two salts of the $[4\text{-}X(py)H]_3Fe_2Cl_xBr_{9-x}$ family (here, X may be Cl, Br or H) which are known to have orthorhombic structures. While the ferromagnetic peak in the susceptibility data is found at 2.00 K, a second maximum at 2.5 K is also found and the critical temperature for long-range order is identified at 2.212 K from the λ-feature in the magnetic specific heat, and a large degree of short-range order is observed. Analysis according to the high-temperature series expansion yields $|J|/k_B = 0.084$ K and $g = 2.02$.

Supplementary material

A table of observed and calculated structure factors for $(pyH)_3Fe_2Cl_9$ (11 pages) is available from the authors.

Acknowledgements

The work in Chicago was supported in part by the Solid State Chemistry Program of the Division of Materials Research of the National Science Foundation, under Grants DMR-8515224 and DMR-8815798. We also thank Basrah University and the Iraqi government for the award of a scholarship. Acknowledgement is made to the Donors of the Petroleum Research Fund, administered by the American Chemical Society, and the BP Venture Research Unit for the partial support of this research.

References

1 R. F. Weinland and A. Kiszling, *Z. Anorg. Chem., 120* (1922) 220.
2 A. Earnshaw and J. Lewis, *J. Chem. Soc.,* (1961) 396.
3 A. P. Ginsberg and M. B. Robin, *Inorg. Chem., 2* (1963) 817.
4 J. A. Zora, K. R. Seddon, P. B. Hitchcock, C. B. Lowe, D. P. Shum and R. L. Carlin, *Inorg. Chem., 29* (1990) 3302.
5 J. C. Deaton, M. S. Gebhard and E. I. Solomon, *Inorg. Chem., 28* (1989) 877.
6 M. L. Hackert and R. A. Jacobson, *Acta Crystallogr., Sect. B, 27* (1971) 1658.
7 C. B. Lowe, R. L. Carlin, A. J. Schultz and C.-K. Loong, *Inorg. Chem., 29* (1990) 3308.
8 R. Shaviv, K. E. Merabet, D. P. Shum, C. B. Lowe, D. Gonzalez, R. Burriel and R. L. Carlin, *Inorg. Chem.,* in press.
9 G. C. Pimental and A. L. McClellan, *The Hydrogen Bond,* W. H. Freeman, San Francisco, CA, 1960, pp. 290–291.
10 C. Rerat, *Acta Crystallogr., 15* (1962) 427.
11 R. L. Carlin, *Magnetochemistry,* Springer, Berlin, 1986.
12 L. J. de Jongh and D. J. Breed, *Solid State Commun., 15* (1974) 1061.
13 J. A. Puertolas, R. Navarro, F. Palacio, J. Bartolome and R. L. Carlin, *Phys. Rev. B, 26* (1982) 395.
14 T. Moriya, in G. T. Rado and H. Suhl (eds.), *Magnetism,* Vol. 1, Academic Press, New York, 1963, pp. 93–96.
15 T. Moriya, *Phys. Rev., 120* (1960) 91.
16 R. L. Carlin, C. B. Lowe and F. Palacio, *An. Quim., 87* (1991) 5.
17 R. Shaviv and R. L. Carlin, *Inorg. Chem., 31* (1992) 710.